Building a digital twin for material testing: Model Reduction and Data Assimilation

Rubén Aylwin[1,*], **Nina Beranek**[1,**], **Gajendra Babu Budihala**[1,**], **Matthias Mettenleiter**[2,***], **Göksu Oruc**[1,**] und **Karsten Urban**[1,**]

[1] Ulm University, Institute of Numerical Mathematics, Helmholtzstr. 20, 89081 Ulm, Germany

[2] ATR Software, Marlene-Dietrich-Str. 5, 89231 Neu-Ulm, Germany

The rapid advancement of industrial technologies, data collection, and handling methods has paved the way for the widespread adoption of Digital Twins (DTs) in engineering, enabling seamless integration between physical systems and their virtual counterparts.

The current work presents a comprehensive framework for building robust and scalable DTs tailored for material testing applications using a Universal Testing Machine (UTM), focusing on core challenges such as model fidelity, data integration, and computational efficiency. Our goal is to build a DT of a material subjected to cyclic loading. A linear elastic material model with its governing Partial Differential Equation (PDE) and discretization through the Finite Element Method (FEM) is considered. The obtained high-fidelity solution is used within the framework of the Reduced Basis Method (RBM) to construct a reduced model with the help of a well-known greedy method, which significantly improves the computational efficiency. The solution is further improved by integrating data collected by sensors in real-time through the Parametrized-Background-Data-Weak (PBDW) method.

The presented approach integrates physical knowledge, which is available in terms of constitutive or material modelling, and real-time sensor data to construct and continuously update the DTs. Emphasis is placed on the knowledge available through PDEs, which address the reliability and robustness of the DT model. This work highlights the advantages of the DTs in predictive maintenance and health monitoring of assets or systems, which eliminates unexpected failures and downtimes in engineering applications.

Danksagung This project is funded by the *Federal Ministry for Economic Affairs and Energy of Germany* (BMWE – Bundesministerium für Wirtschaft und Energie der Bundesrepublik Deutschland). The authors are grateful to Julian Henning (formerly at ATR Software, Neu-Ulm, Germany) for the development, construction, and intense collaboration on the UTM.

1 Introduction

The *Digital Twin* (DT) paradigm has emerged as a cornerstone of Industry 4.0 and beyond, fundamentally reshaping how engineers design, monitor, and maintain physical assets. At its core, a DT is a living, data-driven virtual replica of a physical system that evolves in lockstep with its real-world counterpart, [3]. By fusing real-time sensor data, operational histories along with underlying physics, DTs unlock unprecedented capabilities in performance optimization, anomaly detection, and predictive maintenance, [8].

As an example, in the context of material testing, where understanding fatigue, damage accumulation, and mechanical response under cyclic loading is critical, the DT concept offers transformative potential with the aforementioned outcomes in industry. Standard test rigs can be augmented by DTs to enable continuous, in situ model calibration and real-time structural health assessment to estimate the *remaining useful life* (RUL), [10].

Despite this promise, the practical deployment of robust DTs presents three interrelated challenges: (1) achieving sufficient model fidelity to accurately capture relevant physical phenomena; (2) integrating heterogeneous data sources while maintaining numerical stability and physical consistency; and (3) ensuring computational efficiency to support real-time or near-real-time inference. High-fidelity numerical models based e.g. upon the *Finite Element Method* (FEM) offer detailed resolution of generated stress, local strain concentrations, and boundary effects under cyclic loading, but are computationally expensive and thus impractical for live updates. On the other hand, purely data-driven surrogates are computationally efficient, but may deviate from the governing physics when operating outside their training regime, in the presence of sensor noise, or in the

* Corresponding author: e-mail ruben.aylwin@uni-ulm.de
** e-mail nina.beranek@uni-ulm.de, gajendra.budihala@uni-ulm.de, goeksu.oruc@uni-ulm.de, karsten.urban@uni-ulm.de
*** e-mail matthias.mettenleiter@atr-software.de

presence of even slight changes in the operating conditions, which happen all the time in the real-time scenario. Moreover, such models often lack the required engineering precision and accuracy.

To bridge this gap, we propose a hybrid DT framework for a prototypical material subjected to cyclic tension using a *Universal Testing Machine* (UTM). We begin with a linear elastic constitutive model governed by a *Partial Differential Equation* (PDE), discretized via the FEM to generate high-resolution „snapshots“ of displacement and strain fields across a range of loading amplitudes and cycle counts. These snapshots form a *Reduced Basis* (RB) model, constructed using a greedy-type algorithm. This RB surrogate offers orders-of-magnitude computational acceleration while maintaining a certified error bound relative to the full-order FEM model.

To refine the RB surrogate to real-world observations, we employ the *Parameterized Background Data Weak* (PBDW) method [10, 16] for data assimilation. Within this framework, the RB solution serves as a background approximation, which is continuously corrected using sparse, real-time measurements obtained from strain gauges and extensometers mounted on the specimen. This approach synergistically combines the robustness of physics-based modelling with the adaptability of data-driven updates, yielding a DT that is both accurate under nominal conditions and resilient to unanticipated perturbations.

The primary contributions of this work are threefold: i) A scalable methodology for constructing RB surrogates tailored for cyclic material testing is presented; ii) a PBDW-based data assimilation mechanism that integrates sensor measurements with reduced-order models is shown; and iii) a case study demonstrating the effectiveness of the proposed DT framework on a UTM platform is performed.

The remainder of this paper is organited as follows: Section 2 is devoted to the problem setting and physical model we consider in the current paper; Section 3 details the governing equations and the FE discretization, whereas the reduced-order modeling strategy is presented in Section 4. Section 5 outlines the data assimilation framework and Section 6 presents implementation details and experimental validation; Section 7 is devoted to the presentation of our numerical results and Section 8 concludes with challenges and perspectives on extending the presented framework to nonlinear material behavior.

2 Problem Setting and Physical Model

Predicting the mechanical response and degradation of structural components under cyclic loading is a central task in many engineering domains, including the automotive and aerospace industries, [8], and even for testing benches of vehicles, [9]. Components such as suspension arms, engine brackets, or control mounts are routinely subjected to repeated loading during service, which over time leads to fatigue damage and eventual failure. Laboratory-based material testing provides a standardized way to evaluate the endurance of such material structures under controlled cyclic loading conditions.

A common experimental approach is to use a *Universal Testing Machine* (UTM) to perform tension-compression cycles on standardized specimens. These tests help to characterize properties such as elastic modulus, energy dissipation, and fatigue life under repeated loading, [2]. However, traditional testing procedures typically yield only global measures, for instance, force-displacement or stress-strain curves, and provide little insight into the internal state of the specimen. In particular, they do not capture spatially resolved strain distributions, stress concentrations, or evolving damage indicators. As a result, early signs of failure or localized degradation may go undetected.

Digital Twins (DT) offer a promising solution by fusing simulation and data in real-time to create a continuously updating virtual replica of the physical system. In the context of material testing, a DT enables high-resolution field predictions (e.g., displacement or strain) even from sparse sensor data, supports condition monitoring, and enables better fatigue life estimation. Figure 1 illustrates the DT lifecycle applied to this context, including modeling, data acquisition, and model correction.

In this work, we develop a DT framework for a *Polylactic Acid* (PLA) polymer specimen subjected to cyclic tensile loading using a UTM. The core of the model is a dynamic, three-dimensional linear elasticity formulation, which captures the evolution of displacement and strain under time-dependent loads. The applied load varies only in one direction (typically axial), and even though the 3D formulation is retained to capture transverse effects and boundary-layer phenomena, the material is assumed to be isotropic, which discounts the potential anisotropies in material behavior.

The focus is on the elastic regime, consistent with early fatigue studies where plastic deformation is not yet dominant. This assumption enables us to use linear models for efficient reduced-order modeling and real-time correction via data assimilation, as described below.

3 Linear Harmonic Elastic Material Model and Finite Element Discretization

We consider a three-dimensional linear elastic solid undergoing small deformations and subjected to external cyclic loading. The physical behavior of the specimen is assumed to be governed by the equations of dynamic linear elasticity, where the

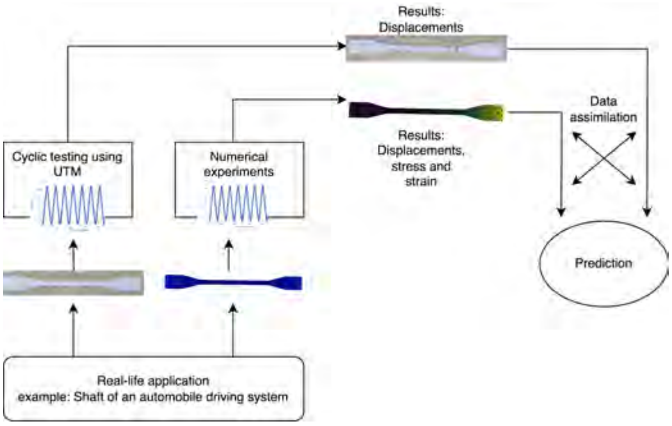

Fig. 1: Digital Twin lifecycle applied to material testing.

displacement field $u : \Omega \times [0, T] \to \mathbb{R}^3$ evolves under external forces and inertia. Here, $\Omega \subset \mathbb{R}^3$ denotes the spatial domain, and $[0, T]$ is the time interval, $T > 0$ being the terminal time. The strong form of the governing equations then reads:

$$\rho\, \ddot{u}(x,t) - \nabla \cdot \boldsymbol{\sigma}(u)(x,t) = \mathbf{f}(x,t), \quad \text{in } \Omega \times (0,T), \tag{3.1}$$

with boundary and initial conditions on the Dirichlet Γ_D and Neumann Γ_N part of the boundary $\Gamma := \partial\Omega = \Gamma_D \dot{\cup} \Gamma_N$, i.e.,

$$u(x,t) = 0, \qquad \text{on } \Gamma_D \times (0,T), \tag{3.2a}$$
$$\boldsymbol{\sigma}(u)(x,t) \cdot \hat{\mathbf{n}} = \mathbf{T}(x,t), \qquad \text{on } \Gamma_N \times (0,T), \tag{3.2b}$$
$$u(x,0) = u_0(x), \quad \dot{u}(x,0) = v_0(x), \qquad \text{in } \Omega. \tag{3.2c}$$

Rather than solving the fully time-dependent dynamic elasticity problem, we exploit the periodic nature of the applied load and adopt a time-harmonic formulation. This allows us to reformulate the second-order evolution problem as a parametrized Helmholtz-type problem in the frequency domain, which significantly reduces the computational complexity while retaining the essential dynamic behavior. We introduce a time-harmonic assumption. Let $p > 0$ denote the load period and $\omega = 2\pi/p$ the angular frequency. We assume

$$u(x,t) = \Re\left[\hat{u}(x)e^{-i\omega t}\right], \tag{3.3}$$

where $\hat{u} : \Omega \to \mathbb{C}^3$ is the complex-valued displacement amplitude. Substituting into the momentum balance and neglecting transients yields the frequency-domain (Helmholtz-type) problem, [1]:

$$-\nabla \cdot \boldsymbol{\sigma}(\hat{u})(x) = \rho\omega^2 \hat{u}(x), \qquad \text{in } \Omega, \tag{3.4a}$$
$$\hat{u}(x) = 0, \qquad \text{on } \Gamma_D, \tag{3.4b}$$
$$\boldsymbol{\sigma}(\hat{u})(x) \cdot \hat{\mathbf{n}} = \hat{\mathbf{T}}(x), \qquad \text{on } \Gamma_N. \tag{3.4c}$$

The stress tensor is defined by:

$$\boldsymbol{\sigma}(\hat{u}) = \lambda\, \mathrm{div}(\hat{u})\, \mathbf{I} + 2\mu\, \boldsymbol{\varepsilon}(\hat{u}), \tag{3.5}$$

with the strain $\boldsymbol{\varepsilon}(\hat{u}) = \frac{1}{2}\left(\nabla\hat{u} + \nabla\hat{u}^\top\right)$, where E is the Young's modulus, ν is the Poisson's ratio and the Lamé parameters λ and μ are given by:

$$\lambda = \frac{E\nu}{(1+\nu)(1-2\nu)} \quad \text{as well as} \quad \mu = \frac{E}{2(1+\nu)}.$$

3.1 Variational Formulation

Let $V := [H^1_{0,\Gamma_D}(\Omega)]^3$ be the space of admissible test and trial functions.[1] The variational (weak) form of the harmonic elasticity problem then amounts to finding $\hat{u} \in V$ such that

$$a(\hat{u}, v) - \rho\omega^2 m(\hat{u}, v) = F(v), \qquad \forall v \in V, \tag{3.6}$$

where the bilinear and linear forms are defined as:

$$a(u,v) := \int_\Omega \boldsymbol{\sigma}(u) : \boldsymbol{\varepsilon}(v)\, dx, \qquad m(u,v) := \int_\Omega u \cdot v\, dx \quad \text{and} \quad F(v) := \int_{\Gamma_N} \hat{\mathbf{T}} \cdot v\, ds. \tag{3.7}$$

[1] By $H^1_{0,\Gamma_D}(\Omega)$ we denote the standard Sobolev space with homogeneous Dirichlet boundary conditions on Γ_D.

3.2 Well-posedness: Existence, Uniqueness and Stability

The variational problem (3.6) is of Helmholtz type and involves a bilinear form that is not coercive but satisfies a Gårding inequality. We recall the classical result for such problems:

Satz 3.1 (Fredholm Alternative for Gårding-type problems e.g. [1, Thm 3.10.5]) *Let $a(\cdot,\cdot)$ be a continuous bilinear form on a Hilbert space V and suppose there exist constants $\alpha > 0$ and $\beta \geq 0$ such that:*

$$a(v,v) + \beta \|v\|^2_{L^2(\Omega)^3} \geq \alpha \|v\|^2_V, \quad \forall v \in V. \tag{3.8}$$

Then the associated variational problem

$$\text{Find } u \in V \text{ such that } a(u,v) = F(v) \quad \forall v \in V, \tag{3.9}$$

has a unique solution for all $F \in V'$ if and only if the corresponding homogeneous problem admits only the trivial solution. Moreover, the solution depends continuously on the data, i.e., $\|u\|_V \leq C\|F\|_{V'}$. □

In our case, the bilinear form reads

$$a_\omega(u,v) := a(u,v) - \rho\omega^2 m(u,v),$$

is continuous and satisfies a Gårding inequality. Provided that the angular frequency ω does not coincide with a resonance frequency (i.e., the kernel of the homogeneous problem is trivial), the solution to (3.6) exists, is unique, and depends continuously on the data (stability). Hence, the problem is well-posed in the Hilbert space $V := [H^1_{0,\Gamma_D}(\Omega)]^3$ and suitable for numerical approximation by the finite element method.

3.3 Finite Element Discretization

Next, we describe a standard FE discretization. To this end, let $\mathcal{T}_h$ be a conforming mesh on Ω with mesh size h. We define the discrete finite element space as

$$V_h := \{v_h \in C^0(\bar{\Omega})^3 \mid v_h|_K \in \mathbb{P}_1(K)^3,\ \forall K \in \mathcal{T}_h,\ v_h = 0 \text{ on } \Gamma_D\}.$$

Standard approximation properties and convergence results for such elements are provided, for example in [1]. The complex-valued displacement field $\hat{u}$ is approximated as:

$$\hat{u}_h(x) = \sum_{i=1}^{N_h} \phi_i(x)\,\hat{\mathbf{U}}_i,$$

where $\{\phi_i\}_{i=1}^{N_h}$ are the nodal basis functions, and $\hat{\mathbf{U}}_i \in \mathbb{C}^3$ are the unknown nodal displacement vectors. Substituting into the variational formulation (3.6) yields the linear system:

$$(\mathbf{K}(\lambda,\mu) - \rho\omega^2\mathbf{M})\hat{\mathbf{U}} = \mathbf{F},$$

where $\mathbf{K} \in \mathbb{R}^{N_h \times N_h}$ is the global stiffness matrix assembled from the bilinear form $a(\cdot,\cdot)$, $\mathbf{M} \in \mathbb{R}^{N_h \times N_h}$ is the mass matrix from $m(\cdot,\cdot)$ and $\mathbf{F} \in \mathbb{R}^{N_h}$ is the global load vector assembled from $F(\cdot)$.

4 Building a Reduced Order Model

In our context, the parameters $\mu = (E,\nu,\rho,\omega)$ as well as loading data are treated as inputs for which rapid online evaluations are required in the sense that given values of μ (e.g. from measurements), the solution $u(\mu)$ of (3.6) is required extremely fast, namely in real-time. We only sketch the main ingredients and refer the reader to [6, 15, 17].

However, the FE discretization of the harmonic elasticity problem introduced above results in a large-scale linear system of the form:

$$(\mathbf{K}(\mu) - \rho(\mu)\omega^2\mathbf{M}(\mu))\hat{\mathbf{U}}(\mu) = \hat{\mathbf{F}}(\mu), \tag{4.1}$$

where $\mu \in \mathcal{P} \subset \mathbb{R}^p$ (here $p = 4$, see above) is a vector of parameters, and $\hat{\mathbf{U}}(\mu) \in \mathbb{C}^{N_h}$ is the complex-valued nodal displacement vector. As above, but now stressing the parameter-dependence of the quantities, the matrices $\mathbf{K}(\mu)$ and $\mathbf{M}(\mu)$ are the stiffness and mass matrices of (large) size $N_h \times N_h$, respectively, and $\hat{\mathbf{F}}(\mu)$ is the parameter-dependent load vector.

While this formulation accurately captures the system dynamics, solving (4.1) for many values of μ (e.g., in a real-time DT setting) is computationally infeasible due to the high dimension N_h of the FE system. To overcome this, we suggest applying model order reduction via the *Reduced Basis Method* (RBM).

4.1 Reduced Basis Approximation and Solution Manifold

Let $\mathcal{M}_h^{\text{bk}} := \{\hat{u}_h(\mu) \in V_h \mid \mu \in \mathcal{P}\}$ denote the (detailed) *solution manifold* of the parameterized PDE. The RBM seeks to approximate the exact solution $\hat{u}(\mu)$ in a low-dimensional subspace $Z_n \subset V_h$, $n \ll N_h$, generated from representative solutions (snapshots) at selected parameter values. We can then write the reduced-order approximation as

$$\hat{u}_n(\mu) = \sum_{i=1}^{n} \alpha_i(\mu)\, \zeta_i, \tag{4.2}$$

where $\{\zeta_i\}_{i=1}^n \subset V_h$ is a reduced basis spanning Z_n (typically with $n \ll N_h$), and $\alpha_i(\mu)$ are the expansion coefficients determined by the Galerkin projection onto Z_n.

4.2 Affine Parameter Dependence and Offline–Online Decomposition

To enable efficient evaluation of the reduced system, we assume that the operators in (4.1) admit an *affine parameter decomposition*:

$$\mathbf{K}(\mu) = \sum_{q=1}^{Q_K} \Theta_K^q(\mu)\, \mathbf{K}_q, \qquad \mathbf{M}(\mu) = \sum_{q=1}^{Q_M} \Theta_M^q(\mu)\, \mathbf{M}_q, \qquad \hat{\mathbf{F}}(\mu) = \sum_{q=1}^{Q_F} \Theta_F^q(\mu)\, \mathbf{F}_q, \tag{4.3}$$

where the functions $\Theta_X^q(\mu)$ are scalar-valued and parameter-dependent, and the matrices $\{\mathbf{K}_q\}, \{\mathbf{M}_q\}, \{\mathbf{F}_q\}$ are parameter-independent and precomputed during an *offline phase*. This separation allows the efficient assembly of the reduced system in an *online phase* without re-accessing the full-order FE mesh.

4.3 Snapshot Generation and the Greedy Algorithm

The reduced basis $\{\zeta_i\}_{i=1}^n$ is generated using the Greedy algorithm. The snapshots $\hat{u}(\mu)$ are determined by the detailed („full-order“) model for selected parameter samples. Let $\Xi_{\text{train}} \subset \mathcal{P}$ be a training set. The algorithm proceeds iteratively:

1. Initialize with an empty basis $Z_0 = \emptyset$.
2. For $i = 1, \dots, n$:
   (a) Identify $\mu^{(i)} \in \Xi_{\text{train}}$ that maximizes a residual-based error indicator $\Delta_i(\mu)$.
   (b) Solve the full-order system (4.1) at $\mu^{(i)}$ to obtain $\zeta_i := \hat{u}(\mu^{(i)})$.
   (c) Possibly orthogonalize the snapshot set to extract dominant modes.
   (d) Enrich the reduced basis space: $Z_i = \text{span}\{Z_{i-1}, \zeta_i\}$.

The orthogonalization step involves computing the singular value decomposition (SVD) of a snapshot matrix and retaining the mode(s) that maximize energy content, based on a prescribed tolerance. The reduced basis is then $\{\zeta_1, ..., \zeta_n\}$ and Z_n is spanned by this basis.

4.4 Reduced System and Computational Benefits

The reduced system is obtained by projecting (4.1) onto Z_n. Let $\mathbf{Z}_n \in \mathbb{R}^{N_h \times n}$ be the matrix whose columns are the reduced basis vectors. The reduced system reads

$$(\mathbf{K}_n(\mu) - \rho(\mu)\, \omega^2\, \mathbf{M}_n(\mu))\, \boldsymbol{\alpha}(\mu) = \mathbf{F}_n(\mu), \tag{4.4}$$

where the reduced components $\mathbf{K}_n(\mu), \mathbf{M}_n(\mu) \in \mathbb{R}^{n\times n}$ and $\mathbf{F}_n(\mu) \in \mathbb{R}^n$, are given by

$$\mathbf{K}_n(\mu) = \mathbf{Z}_n^\top \mathbf{K}(\mu)\mathbf{Z}_n, \quad \mathbf{M}_n(\mu) = \mathbf{Z}_n^\top \mathbf{M}(\mu)\mathbf{Z}_n, \quad \mathbf{F}_n(\mu) = \mathbf{Z}_n^\top \hat{\mathbf{F}}(\mu). \tag{4.5}$$

This system is of much smaller dimension $n \ll N_h$ and can be solved in real-time, enabling fast predictions across a wide range of parameter values.

4.5 Limitations of Reduced Models

Despite RBMs offering computational efficiency, they are not immune to limitations. In particular, the reduced basis is constructed based on a finite training set and idealized physics. As a result, the reduced solution may be unable to address errors and outliers resulting from the presence of modeling errors, sensor noise, or operational changes that were not captured in the training data. In the context of DT, this lack of robustness can limit the trustworthiness of the model, especially when sensor data are abundant from real experiments. To address this, we can take advantage of the data assimilation technique, which is introduced in the next section, that dynamically corrects the reduced model using real-time observations.

Moreover, the RBM is a *linear* model reduction technique as it projects the original model onto a low-dimensional space. It is known that such a linear reduction technique works well if the state depends smoothly on the parameter, which is, e.g. the case for elliptic and parabolic problems, [13,17]. However, the error may decay very slowly for increasing sizes of the reduced model for transport- and wave-type phenomena, [4, 13].

5 Data Assimilation via the Parametrized-Background-Data-Weak (PBDW) Method

While *reduced-order models* (ROMs), such as those built by the RBM via the Greedy algorithm, provide efficient surrogates for high-fidelity simulations, they are fundamentally predictive. These models depend on a *best-knowledge* (bk) description [12, 14, 18] of the system, including governing PDEs, boundary conditions, and constitutive laws, and they are also sensitive to modeling errors, parameter uncertainties, and unmodeled physical effects. In the DT context, this mismatch can result in significant deviations between model predictions and sensor observations.

To mitigate these discrepancies, we adopt the *Parametrized-Background-Data-Weak* (PBDW) framework, [5, 10, 16]. This method enables online correction of reduced models by assimilating real-time sensor data. It views the reduced-order model as a parameterized background field and augments it with a data-driven correction to produce an improved solution that is both physics-informed and observation-consistent.

5.1 Problem Setting and Decomposition

Let $\mathcal{H}$ denote the Hilbert space in which the solution lives, e.g. $\mathcal{H} = H^1_{0,\Gamma_D}(\Omega)^3$. Let $Z_n \subset \mathcal{H}$ be the RB space obtained via the above-described greedy method on the high-fidelity harmonic model. Let $U_m \subset \mathcal{H}$ be a (reduced) observation space built from the available sensor configuration. The goal is to reconstruct the true displacement field $\hat{u}^{\text{true}}$ (the complex amplitude in the time-harmonic model) via the PBDW decomposition

$$\hat{u}^{\text{true}} \approx \hat{u}^{\text{PBDW}} := z + \eta, \quad \text{with } z \in Z_n,\ \eta \in U_m, \tag{5.1}$$

where z represents the background (ROM) prediction and η is a corrective field inferred from sensor data.

Since the underlying PDE is harmonic in time, we assume that the displacement field admits the form

$$u(x,t) = \Re\left[\hat{u}(x)e^{-i\omega t}\right],$$

and measurements are sampled over time. The observed data $y_j(t)$ are therefore modeled as

$$y_j(t) \approx \ell_j(\hat{u}) \cdot \Re(e^{-i\omega t}),$$

and data assimilation is carried out on the complex-valued spatial amplitude $\hat{u}$.

We assume the availability of $\mathbb{N} \ni M \geq m$ real-time sensor measurements, modeled as noisy bounded linear functionals:

$$y_k = \ell_k(\hat{u}^{\text{true}}) + \epsilon_k, \quad k = 1, \dots, M, \tag{5.2}$$

where $\ell_k \in \mathcal{H}'$ and ϵ_k denotes additive sensor noise. To ensure that these functionals are well-defined on $\mathcal{H}$, and to reflect practical sensing physics (e.g., strain gauges or extensometers), we define the sensor functionals as smoothed spatial integrals (see also [5]) by

$$\ell_k(u) := C_k \int_\Omega \exp\left(-\frac{\|x - x_k\|^2}{2\,r_w^2}\right) u(x)\,dx, \tag{5.3}$$

where $x_k \in \Omega$ is the location of the k-th sensor, r_w is the sensor's spatial support radius, and C_k is a normalization constant.

5.2 Variational Formulation

The PBDW approximation $\hat{u}^{\text{PBDW}} = z + \eta$ is obtained by solving the following minimization problem:

$$\min_{z \in Z_n,\, \eta \in U_m} \left\{ \sum_{j=1}^{M} \left|\ell_j(z+\eta) - y_j\right|^2 + \zeta \|\eta\|^2_{\mathcal{H}} \right\}, \tag{5.4}$$

where $\zeta > 0$ is a regularization parameter balancing measurement fidelity and correction smoothness. The first term enforces consistency with measured data, while the second penalizes overfitting by regularizing the correction in the $\mathcal{H}$-norm.

In the limiting cases, as $\zeta \to 0$, the solution tends to interpolate the data exactly (risking instability). As $\zeta \to \infty$, the correction is suppressed and the estimate reverts to the background field z.

Satz 5.1 (Well-posedness of the PBDW problem [10]) *Let $\mathcal{H}$ be a Hilbert space, $Z_n \subset \mathcal{H}$ a reduced subspace, $U_m \subset \mathcal{H}$ an observation space, and $\{\ell_k\}_{k=1}^M \subset \mathcal{H}'$ a set of linearly independent bounded linear functionals. Then, for any data $y = (y_1, \ldots, y_M) \in \mathbb{R}^M$ and regularization parameter $\zeta > 0$, the PBDW problem* (5.4) *admits a unique minimizer $u^{PBDW} = z + \eta \in Z_n + U_m$.* □

5.3 Construction of the Observation Space

Let $\{x_k\}_{k=1}^M \subset \Omega$ be the sensor locations. We construct basis functions $\{\psi_k\}_{k=1}^M \subset \mathcal{H}$ satisfying:

$$\ell_j(\psi_k) = \delta_{jk}, \quad \text{for } j, k = 1, \ldots, M, \tag{5.5}$$

i.e., each ψ_k is dual to the k-th functional and serves to interpolate corrections in the vicinity of sensor x_k. In practice, ψ_k may be defined using Gaussian radial basis functions, local finite element bubble functions, or empirical interpolation modes. The correction field is then given by:

$$\eta = \sum_{k=1}^{M} \beta_k \psi_k,$$

with the coefficients β_k determined by solving the minimization problem (5.4). This construction ensures that PBDW corrections are localized and consistent with the available sensing configuration, while remaining physically meaningful in the variational framework.

5.4 Data Assimilation by PBDW in the Digital Twin Framework

In our DT implementation, the background field $z(\mu) \in Z_n$ is computed from the reduced-order model for a given input μ. Sensor observations y_k are then used to compute the PBDW-corrected field $\hat{u}^{\mathrm{PBDW}}$. This results in an updated state estimate that reflects both the best knowledge of physics and the most recent measurements.

The PBDW method enables the real-time assimilation of sparse and noisy data, resulting in improved accuracy and robustness, particularly when the model deviates from reality due to aging, loading variations, or environmental effects. By dynamically blending physics and data, PBDW closes the loop in the DT, transforming it from a passive simulator into an adaptive, real-time predictive engine.

The observation points x_k and the reduced update space U_m are also constructed in a greedy manner following [11, 16].

6 Experimental Setup and Results

To validate the proposed DT framework, we conduct cyclic loading tests on a custom material testing setup using a *Universal Testing Machine* (UTM), as shown in Figure 2. The test rig was designed and assembled in-house using 3D-printed components as shown in Figure 3, including the specimen grips and fixture supports. The test specimen itself is 3D-printed using *Polylactic Acid* (PLA), a commonly used thermoplastic polymer with moderate strength and stiffness characteristics suitable for laboratory-scale fatigue studies. Given the additive manufacturing constraints and the structural limitations of the

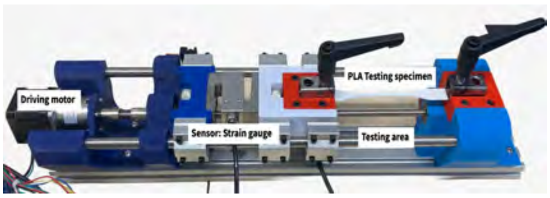

Fig. 2: Universal testing machine, originally constructed by J. Henning (formerly at ATR Software, Neu-Ulm (Germany).

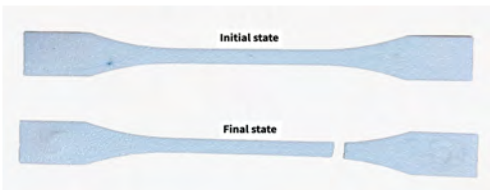

Fig. 3: 3D printed testing Specimens, before and after the testing.

printed fixtures, the test configuration is limited to applying uniaxial tensile loads only. Compression loading is avoided due to stability issues and the risk of buckling or fixture damage.

To simulate the material's fatigue behavior, the specimen is subjected to repeated asymmetric cyclic tensile loading with an amplitude of 200 N. The load is applied over an approximately 21-second interval per cycle series, and the process is repeated until the specimen exhibits irreversible plastic deformation or complete failure. The specimens are shown in Figure 3 before and after their fracture.

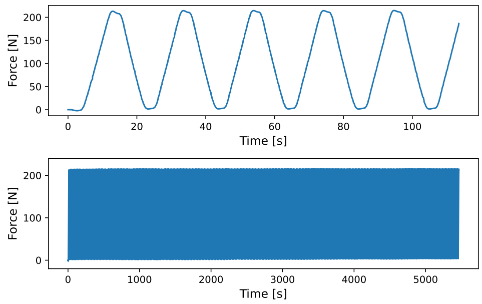

Fig. 4: Amplitude of force.

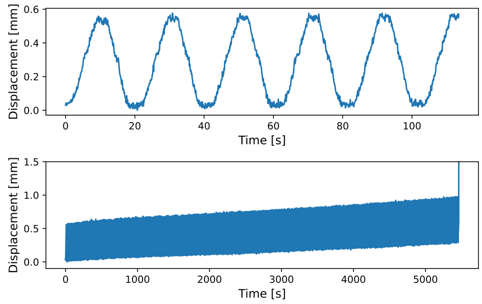

Fig. 5: Displacement measured from the strain gauge.

Figure 4 shows the applied force over time, and the corresponding displacement response of the specimen is shown in Figure 5. These measurements are acquired in real-time using the UTM's internal load cell and displacement transducer. The collected sensor data serves two purposes: (i) to calibrate the reduced-order model offline, and (ii) to perform online data assimilation using the PBDW method for state correction and health estimation.

7 Numerical Results

In this section, we present results of some of our numerical experiments.

7.1 Finite Element Method

For the implementation of the linear elasticity equations and their finite element discretization, we employ the open-source finite element library FEniCSx, [19, 20]. As described in Section 3.3, we use piecewise linear finite elements ($\mathbb{P}_1$) on meshes generated with Gmsh, [21]. Figure 6 illustrates the geometry of the specimen used for the numerical experiments from two different perspectives.

To validate the correctness of the finite element implementation, we consider a Dirichlet problem with a known analytical solution. Specifically, we solve the variational formulation given by (3.6), with the forcing functional defined as $F(v) := \int_\Omega f \cdot v \, dx$ and with Dirichlet boundary conditions $u = g$ prescribed on the entire boundary, i.e., $\Gamma_D = \partial\Omega$ and $\Gamma_N = \emptyset$. The data is chosen as $g(x) := [(x_1 + 7.5 \times 10^{-2})^2,\ 0,\ 0]^\top$, $f(x) := [-2 - 2(x_1 + 7.5 \times 10^{-2})^2,\ 0,\ 0]^\top$ and the Lamé parameters are set to $\lambda = 0.5$ and $\mu = 0.25$. For this setting, the exact solution reads $u(x) = [(x_1 + 7.5 \times 10^{-2})^2,\ 0,\ 0]^\top$.

Figure 7 shows the convergence of the finite element solution towards the analytical reference. As expected for linear finite elements, we observe first-order convergence with respect to the mesh size indicating that our code is reliable.

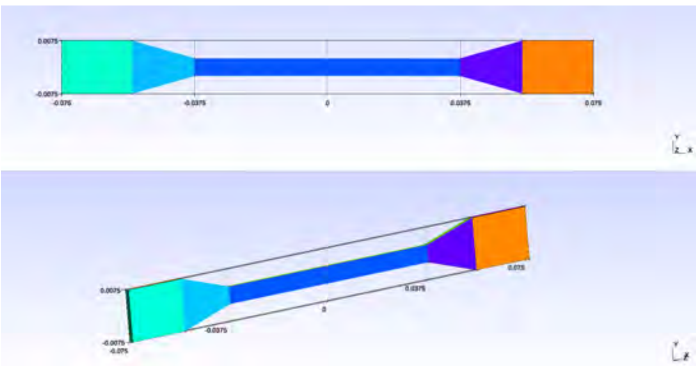

Fig. 6: Geometry of the specimen (distances in meters). Axes on the bottom right indicate the corresponding perspectives.

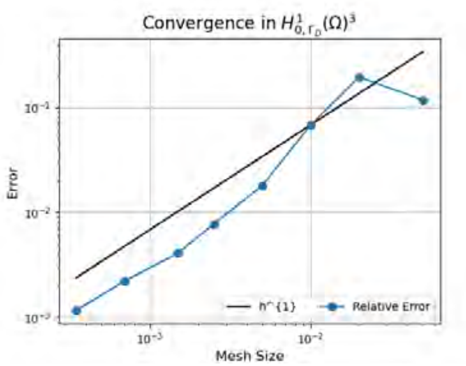

Fig. 7: Relative error achieved by the FE discretization of the equations of linear elasticity with Dirichlet boundary conditions.

7.2 Reduced Basis

The FE code is used as a backbone for model reduction in the sense that the snapshots selected by the greedy algorithm (see Section 4) are computed by this full-order system using a mesh with characteristic size $h \approx 10^{-3}$. The greedy method itself is based upon minimizing a residual-based error estimator consisting of the product of the inverse of the coercivity constant (which is computable here) and the dual norm of the residual computed by solving corresponding Riesz problems. The snapshots are then orthogonalized and possibly only the most energetic modes are kept.

The implementation is carried out using the library `pyMOR`, [22], which provides efficient tools for model order reduction and offline–online decomposition. In our parametric model, we consider the material density ρ and the Young's modulus E as input parameters. While the density is treated as a fixed constant throughout the domain, the Young's modulus is allowed to vary spatially, reflecting inhomogeneities or material imperfections. In particular, we define $E(x)$ as:

$$E(x) := \begin{cases} E_1, & \text{if} \quad x_1 \leq -0.0375, \\ E_2 & \text{if} \quad -0.0375 < x_1 < 0.0375, \\ E_3, & \text{if} \quad x_1 > 0.0375. \end{cases}$$

These variations are incorporated into the parameter space $\mathcal{P} \subset \mathbb{R}^3$ ($\mu = (E_1, E_2, E_3)^\top$) and are sampled accordingly during the offline stage of the greedy algorithm. This enables us to account for stochastic factors such as material inhomogeneities and manufacturing defects that may occur in different regions of the specimen (see Figure 6 for details on the geometry of the sample). We adopt the following material parameters corresponding to PLA:

$$\nu = 0.35, \quad \lambda = \frac{\nu}{(1-2\nu)(1+\nu)}, \quad \mu = \frac{1}{2(1+\nu)}, \quad E = 2.5 \times 10^9 \text{ Pa}, \quad \text{and} \quad \rho = 1380\frac{kg}{m^3}.$$

Moreover, the time period of the applied cyclic load is set to $T = 20$ seconds.

Figure 8 illustrates the convergence of the reduced basis, where we plot the error of the RB approximation on a test set $\mathcal{P}_{\text{test}} \subset \mathcal{P}$ over the dimension n of the reduced model. We observe exponential convergence, reaching the prescribed tolerance of $\varepsilon = 10^{-4}$ with a reduced dimension of $n = 11$, which shows the enormeous potential for computational speedup needed for the realization of a DT.

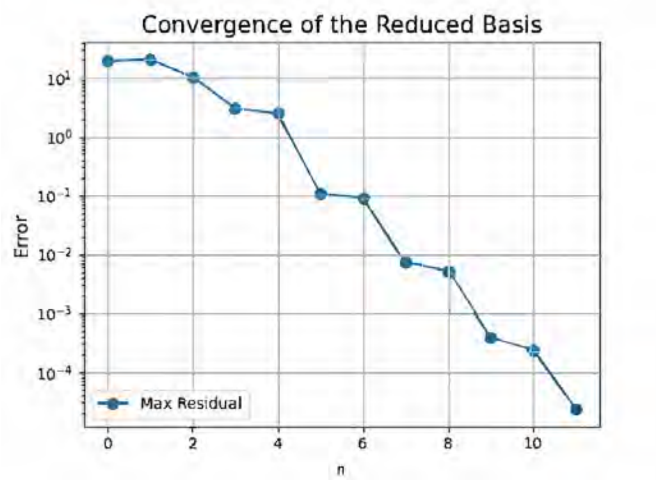

Fig. 8: Convergence of the Reduced Basis obtained through pyMOR: error over size of the reduced model in semilogarithmic scale.

7.3 PBDW and monitoring

Finally, we present numerical results for data assimilation using the PBDW framework based upon displacement measurements acquired in real-time. As described in Section 6, the specimen is subjected to a periodic tensile force with a peak amplitude of 200 N and a time period of 20 seconds. Displacement data is recorded at a single spatial location, $x_{\text{meas}} = [6.4 \times 10^{-2},\ 0,\ 7.5 \times 10^{-3}]^\top$. Given the minimal number of available measurements, the PBDW update is performed in two steps per loading cycle:

1. At times $T = n \cdot 20\,\text{sec}$, for $n \in \mathbb{N}$ (after one cycle, i.e., when the external force vanishes), a first PBDW correction is computed. At this instant, the background model predicts zero displacement, so the measurement is fully represented by the observation space U_m.
2. At subsequent times of interest, the background solution combines the displacement recovered in step one with contributions from the reduced space Z_n.

This approach is motivated by the assumption that the model error largely arises from small permanent deformations not captured by the linear background model. Since only a single measurement is available, the observation space is one-dimensional

($m = 1$), resulting in particularly simple PBDW updates. Since $n \leq m$ (due to the fact that we project the data onto a background space of dimension n), we also get $n = 1$. Hence, U_m and Z_n consist of only one single element each, $m = n = 1$. Figures 9 and 10 display this single element ζ_1 of Z_1, and its axial stress. Moreover, Figures 11 and 12 display the single element of U_1 and its axial stress (in the figures, the functions have been scaled so as to have unit displacement at the measurement point).

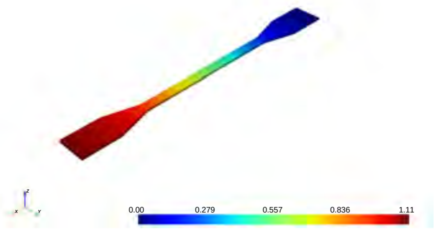

Fig. 9: Sinlge element $\zeta_1 \in Z_1$.

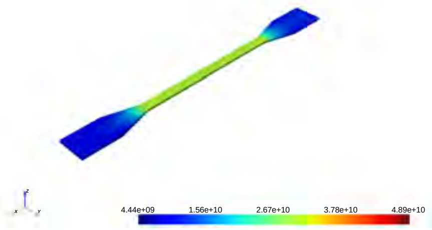

Fig. 10: Axial stress of $\zeta_1 \in Z_1$.

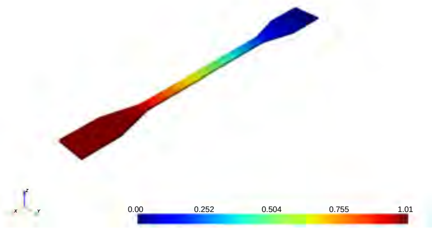

Fig. 11: Single element of U_1.

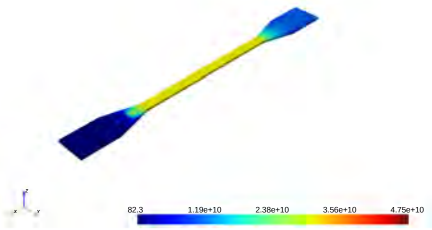

Fig. 12: Single element of U_1: Axial stress.

Having estimated the displacements, we monitor the axial stress at previously specified observation points. In our case, we measure the stresses at $x_{\text{obs}}^{(1)} = [-0.0375, 0, 0]$, $x_{\text{obs}}^{(2)} = [0.0375, 0, 0]$ and $x_{\text{obs}}^{(3)} = [0, 0, 0]$, corresponding to the points in the specimen where high stresses are expected. Figures 13 and 14 show the measured and estimated displacements (on the measurement point x_{meas}) and stresses on the observation points, respectively. The projected displacements show an increasing deviation from the measurements as time goes on, indicating that the current model cannot completely approximate the observed behavior. Furthermore, the current model is unable (by itself) to model highly complex phenomena such as material fatigue.

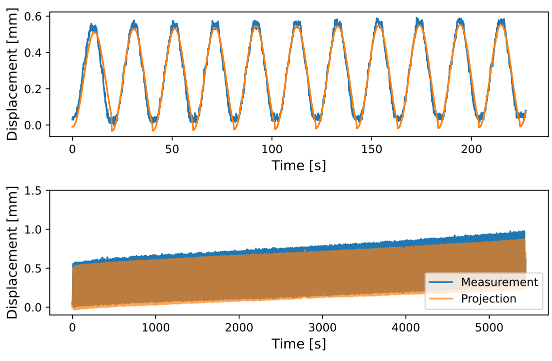

Fig. 13: Comparison between measured and projected displacements.

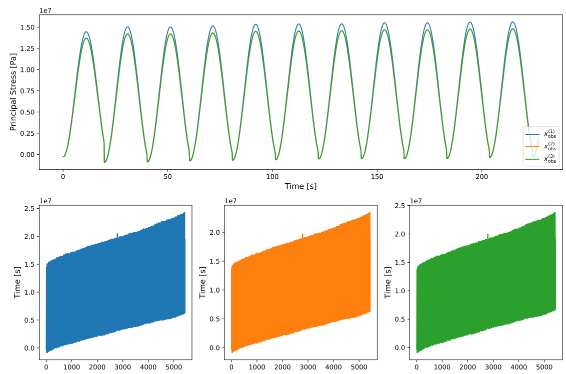

Fig. 14: Projected stresses on the observation points.

These results, when combined with fatigue evaluation methods such as Miner's rule [23] or other damage accumulation models, provide a pathway for estimating the remaining useful life (RUL) of the specimen. In addition, the projected displacements reveal a progressive deviation from the measured data over time, suggesting that the current model, despite data assimilation, cannot fully capture the observed (nonlinear) behavior. This limitation highlights the challenge of modeling long-term degradation phenomena such as fatigue with a purely linear elastic background model.

8 Conclusions and Outlook

We have presented a general framework for constructing a Digital Twin (DT) environment for material testing using a Universal Testing Machine (UTM). The approach is built upon a linear elasticity model, discretized via the Finite Element Method (FEM), which serves as the high-fidelity background model and can be solved to arbitrary accuracy. To enable real-time predictive capability, we apply model order reduction using the Reduced Basis Method (RBM), significantly reducing computational cost while retaining essential parametric dependencies. To incorporate real-time measurement data into the simulation framework, we employ the Parameterized-Background-Data-Weak (PBDW) method for data assimilation. This hybrid strategy allows us to combine physics-based reduced models with sparse sensor observations, yielding displacement and stress field estimates that adapt dynamically to observed behavior.

Even though the presented methodology can be seen as a general road towards building DTs for material testing, we observe some challenges that we will address in future research:

- The linear model cannot fully resolve plastic deformations even when coupled with data – the overall model remains linear.
- We have only a very limited amount of data available. For a full application within a test bench, we see that much more data is required in order to update a background model sufficiently well.
- One goal of a DT within material testing might also be the forecast of the material health, and in particular fatigue and material failure. As those physical quantities can typically not be deduced from numerical predictions, we will also develop a learning method to fill this gap.

Literatur

[1] A. Ern and J. L. Guermond, *Theory and Practice of Finite Elements*, Applied Mathematical Sciences, Vol. 159, Springer (2004).

[2] M. E. Chenthil, S. Praneeth, D. Anand, and M. Srikanth, Universal Testing Machine, Int. J. Res. Technol. **9**, issue 1, pp. 1572–1575 (2022).

[3] S. Farah, D. G. Anderson, and R. Langer, Physical and mechanical properties of PLA, and their functions in widespread applications — A comprehensive review, Adv. Drug Deliv. Rev. **107**, pp. 367–392 (2016).

[4] C. Greif and K. Urban, Decay of the Kolmogorov N-width for wave problems. Appl. Math. Lett., **96**, pp. 216–222 (2019).

[5] W. Haik, Y. Maday, and L. Chamoin, A real-time variational data assimilation method with data-driven model enrichment for time-dependent problems Comput. Methods Appl. Mech. Eng. **405**, no. 115868 (2023).

[6] J. S. Hesthaven, G. Rozza, and B. Stamm. *Certified Reduced Basis Methods for Parametrized Partial Differential Equations*, Springer, 2016.

[7] M. G. Kapteyn, J. V. R. Pretorius, and K. E. Willcox, A probabilistic graphical model foundation for enabling predictive digital twins at scale, Nat. Comput. Sci. **1**, no. 5, pp. 337–347 (2021).

[8] M. G. Kapteyn, D. J. Knezevic, D. B. P. Huynh, M. Tran, and K. E. Willcox, Data-driven physics-based digital twins via a library of component-based reduced-order models, Int. J. Numer. Methods Eng. **123**, no. 13, pp. 2986–3003 (2022).

[9] L. Kopp, L. Steidle, J.-N. Molan, and M. Kley, Development and Discussion of a Virtual Sensor for Stationary Torque Prediction in Electric Machines, IEEE Sens. J. **25**, no. 9, pp. 15216–15223 (2025).

[10] Y. Maday, A. T. Patera, J. D. Penn, and M. Yano, A parameterized-background data-weak approach to variational data assimilation: formulation, analysis, and application to acoustics, Int. J. Numer. Methods Eng. **102**, no. 5, pp. 933–965 (2015).

[11] Y. Maday, A. T. Patera, J. D. Penn, and M. Yano, PBDW State Estimation: Noisy Observations; Configuration-Adaptive Background Spaces; Physical Interpretations, ESAIM Proc. **50**, pp. 144–168 (2015).

[12] R. Milani, A. Quarteroni, and G. Rozza, Reduced basis method for linear elasticity problems with many parameters, Comput. Methods Appl. Mech. Eng. **197**, no. 51–52, pp. 4812–4829 (2008).

[13] M. Ohlberger and S. Rave, Reduced basis methods: Success, limitations and future challenges. Proceedings of the Conference Algoritmy, http://www.iam.fmph.uniba.sk/amuc/ojs/index.php/algoritmy/article/view/389, pp. 1–12 (2016).

[14] C. Prud'homme, D. V. Rovas, K. Veroy, L. Machiels, Y. Maday, A. T. Patera, and G. Turinici, Reliable real-time solution of parametrized partial differential equations: Reduced-basis output bound methods, J. Fluids Eng. **124**, no. 1, pp. 70–80 (2002).

[15] A. Quarteroni, A. Manzoni, and F. Negri. *Reduced basis methods for partial differential equations: An introduction*. Springer, 2016.

[16] T. Taddei, *Model order reduction methods for data assimilation; state estimation and structural health monitoring*, Ph.D. thesis, Massachusetts Institute of Technology (2017).

[17] K. Urban, The Reduced Basis Method in Space and Time: Challenges, Limits and Perspectives, in: Model Order Reduction and Applications, M. Falcone and G. Rozza (eds.), Cetraro 2021, C.I.M.E. Series, Springer, pp. 1–73 (2023).

[18] K. Veroy, *Reduced-basis methods applied to problems in elasticity: Analysis and applications*, Ph.D. thesis, Massachusetts Institute of Technology (2003).

[19] I. A. Baratta, J. P. Dean, J. S. Dokken, M. Habera, J. Hale, C. N. Richardson, M.E. Marie, M. W. Scroggs, N. Sime, and G. N. Wells, *DOLFINx: The next generation FEniCS problem solving environment*, Preprint (2003). doi.org/10.5281/zenodo.10447666

[20] M. S. Alnaes, A. Logg, K. B. Ølgaard, M. E. Rognes, and G. N. Wells, *Unified form language: A domain-specific language for weak formulations of partial differential equations*, ACM T. Math. Software **40**, no. 2, pp. 1-37 (2014).

[21] C. Geuzaine, and J. F. Remacle, *Gmsh: A 3-D finite element mesh generator with built-in pre-and post-processing facilities*, Int. J. Numer. Methods Eng. **79**, no. 11, pp. 1309-1331 (2009).

[22] R. Milk, S. Rave, and F. Schindler, *pyMOR - Generic Algorithms and Interfaces for Model Order Reduction*, SIAM J. Sci. Comput., **38**, no. 5, pp. S194–S216 (2016).

[23] J. Schijve, *Fatigue of Structures and Materials*. Springer, 2008.